Desalination 595 (2025) 118314

Contents lists available at ScienceDirect

Desalination

journal homepage: www.elsevier.com/locate/desal

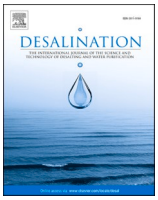

Thermo- and light responsive microgels for efficient brackish and seawater forward osmosis desalination

Amir Jangizehi [a,*], Jan Eckhardt [a], Karolina Izabela Borkowska [a], Zsolt Dallos [a,b], Melanie Bauer [a], Hasan Salehi [c], Reza Razavi [c], Alireza Shakeri [c], Seyed Abdollatif Hashemifard [d], Sebastian Seiffert [a,*]

[a] Department of Chemistry, Johannes Gutenberg University of Mainz, Duesbergweg 10–14, 55128 Mainz, Germany
[b] Department of Materials and Geoscience, Technical University of Darmstadt, 64287 Darmstadt, Germany
[c] School of Chemistry, College of Science, University of Tehran, 14155-6619 Tehran, Iran
[d] Sustainable Membrane Technology Research Group (SMTRG), Water research institute (WRI), Faculty of Petroleum, Gas and Petrochemical Engineering (FPGPE), Persian Gulf University, 75169-13798 Bushehr, Iran

HIGHLIGHTS

- Core-shell poly(NiPAAm-*ran*-SA) microgels are synthesized for efficient desalination.
- Graphene oxide enables partial heating with UV/sunlight, optimizing water recovery.
- Microgels are used in dried and dispersed states for desalination of brackish and seawater.
- Efficient water separation is achieved above microgels' transition temperature.
- System achieves 4.79 LMH in FO and 36 LMH in microfiltration under 2–4 bar pressure.

GRAPHICAL ABSTRACT

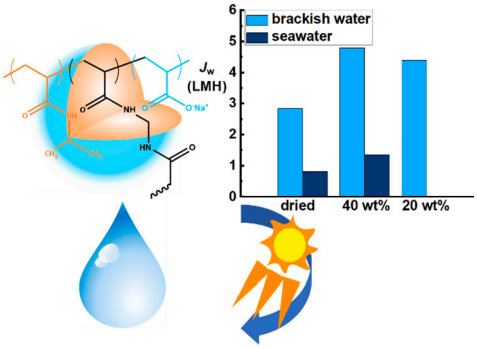

ARTICLE INFO

Keywords:
Thermo-responsive hydrogels
Core-shell microgels
Light responsive microgels
Forward osmosis desalination

ABSTRACT

Forward osmosis desalination presents a promising solution to address water shortages in areas near brackish or seawater sources. This study investigates the use of thermo-responsive poly(*N*-isopropyl acrylamide-*rand*-sodium acrylate) microgels as innovative draw agents for forward osmosis desalination. The drawing ability and responsiveness of these microgels are significantly influenced by the charged comonomer content. Unlike bulk hydrogels, these microgels, owing to their core-shell morphology, maintain thermo-responsivity even at higher comonomer content. Incorporating graphene oxide as a light absorber allows for partial heating, required to reach the transition temperature, to be obtained using UV light radiation. In forward osmosis, microgels can be used either in a dried state or as a concentrated aqueous dispersion. A sample with 25 mol% charged units achieved a balance between water flux and responsiveness. It reached fluxes of 2.84, 4.79 and 4.39 $L{\cdot}m^{-2}{\cdot}h^{-1}$ for the dried state, 40 wt% and 20 wt% dispersions, respectively, when tested with 5 $g{\cdot}L^{-1}$ brackish water. Furthermore, a 40 wt% dispersion drew 35 $g{\cdot}L^{-1}$ seawater at a flux of 1.36 $L{\cdot}m^{-2}{\cdot}h^{-1}$. This sample, which contains graphene oxide, exhibited a volume phase transition temperature at 41 °C that can be achieved through

* Corresponding authors.
E-mail addresses: amir.jangizehi@uni-mainz.de (A. Jangizehi), sebastian.seiffert@uni-mainz.de (S. Seiffert).

https://doi.org/10.1016/j.desal.2024.118314
Received 10 August 2024; Received in revised form 29 October 2024; Accepted 12 November 2024
Available online 13 November 2024

UV light radiation or natural sunlight exposure. Water separation from the microgels was accomplished through filtration under UV-light radiation with a power of 4 $kW{\cdot}m^{-2}$, at 2–4 bar pressure, with a microfiltration membrane and a flux of 36 $L{\cdot}m^{-2}{\cdot}h^{-1}$. These findings highlight the potential of these thermo-responsive microgels for efficient forward osmosis desalination.

1. Introduction

Water scarcity remains one of the most pressing global challenges, with nearly one-third of the world's population lacking adequate access to fresh water for their daily needs [1]. Given that seas and oceans cover more than 95 % of the Earth's surface, water desalination emerges as a viable solution to this crisis [2]. Presently, the primary desalination methods include reverse osmosis (RO) and multi-stage flash evaporation, which collectively deliver fresh water with capacities exceeding 75 million cubic meters per day. Over the past few decades, significant advancements in RO technology have been made, aiming to reduce energy consumption and lower the cost of the final product [3–6]. Currently, forward osmosis (FO), a process already well-established in the food industry, has gained attention as a potential alternative for water desalination [7–11]. The key advantage of the FO process over its RO counterpart lies in its use of a draw agent, which generates the osmotic pressure required to drive water through a semi-permeable membrane, rather than relying on external pressure. The draw agent, with its higher osmotic pressure compared to the feed solution, enables water transport through the membrane. However, this advantage also introduces a significant challenge in forward osmosis desalination: the separation of purified water from the draw agent. An ideal draw agent must not only possess high osmotic pressure to effectively draw water but also facilitate the easy release of water. In recent years, a variety of draw agents have been proposed and investigated, including inorganic salts, polymers, organic molecules, nanoparticles, metathesis precipitable salts, soluble gases or volatile liquids, the NH_3-CO_2 combination, and thermally responsive organic compounds. Each type of draw agent offers distinct advantages and disadvantages, which continue to be the subject of extensive research and development [12].

Polymeric hydrogels have recently emerged as promising candidates for use as draw agents in forward osmosis desalination [13–16] due to their distinctive properties, particularly their ability to absorb water and undergo significant swelling and deswelling in response to specific conditions [17]. The effectiveness of these hydrogels in absorbing water and the conditions necessary for water release are highly dependent on the chemical composition, structural morphology, and molecular architecture of the hydrogel network [17,18]. Compared to conventional draw solutions like 1 M NaCl, hydrogels exhibit limited performance in terms of water absorption through semi-permeable membranes [12]. This subpar performance is also evident in superabsorbent materials, such as poly(sodium acrylate), PSA, which has the capacity to absorb water in amounts ranging from 25 to 600 times its own weight, depending on its crosslinking density. The relatively low water flux observed can be attributed to several factors, including internal polarization effects, slow kinetics of water diffusion within the gels, or inadequate contact between the solid gels and the membranes. Furthermore, PSA hydrogels lack stimuli-responsiveness, and their shrinking process necessitates the application of high pressure. In contrast, stimuli-responsive hydrogels, such as thermo-responsive variants, present a more intriguing alternative.

A well-established example of thermo-responsive hydrogels is poly (*N*-isopropyl acrylamide) (PNiPAAm), which exhibits shrinkage when heated above 34 °C. Despite this notable thermo-responsiveness, PNiPAAm hydrogels generally demonstrate poorer water flux compared to PSA hydrogels, primarily due to their relatively lower osmotic pressure [19]. Achieving an effective balance between water flux and water release, two essential characteristics of an efficient draw agent, can be accomplished by using hydrogels that blend high water absorption capacity with stimuli-responsiveness to enable efficient water release. In this context, hydrogels incorporating both sodium acrylate (SA) and NiPAAm units have been explored as potential draw agents with well-balanced properties. [19] In these hydrogels, SA predominantly influences the water flux, while NiPAAm governs the water release capacity. However, the introduction of charged groups tends to diminish the shrinkage ability of the hydrogels due to alterations in the balance between hydrophilic and hydrophobic components within NiPAAm [20–22]. Our preliminary research indicates that incorporating just 5 mol% of SA units can shift the volume phase transition temperature (VPTT) of NiPAAm hydrogels from 34 °C to 50 °C. With 10 mol% SA, the VPTT is not observed even at temperatures as high as 60 °C [23]. To address this challenge, a feasible solution involves transitioning from a random copolymer architecture to alternative structures such as block copolymers, (semi)interpenetrating networks, or core-shell configurations. These alternative morphologies reduce the interaction between charged and responsive components compared to random copolymer structures, thereby allowing a higher concentration of SA units in the hydrogel network while still maintaining thermo-responsiveness.

Cai et al. reported on a semi-interpenetrating network of NiPAAm SA containing 20 mol% linear PSA, which demonstrated a remarkable water release of more than 90 % upon heating above 40 °C. [24] In contrast, in that work, a hydrogel created by random copolymerizing of 20 mol% SA with 80 mol% NiPAAm did not exhibit any water release, despite having an equilibrium swelling ratio comparable to that of the semi-interpenetrating network counterpart. This discrepancy underscores the significant impact of hydrogel architecture on its water release properties. Additionally, Hartanto et al. explored the performance of P(NiPAAm-*ran*-SA) microgels synthesized through surfactant-free emulsion polymerization at 70 °C [25]. This process results in microgels with sizes in the range of several hundred nanometers. At the polymerization temperature, the PNiPAAm component is above its VPTT and thus contracts, while the PSA component does not exhibit the same behavior. Consequently, these microgels exhibit a core-shell morphology, with the core predominantly composed of NiPAAm units and an outer shell of SA [26,27]. The findings of Hartanto et al. indicated that the shrinkage capability of these microgels is minimally affected by the presence of SA units, up to an 8 mol% content, with water release remaining within the range of 90–94 % at 40 °C. Conversely, the inclusion of SA units significantly enhances the initial water flux of the microgels, achieving more than a threefold increase compared to pure PNiPAAm microgels.

A key advantage of these sub-micrometer microgels is their ability to disperse uniformly in water. This characteristic allows for the use of both the dried and dispersed forms of the gel as draw agents. Furthermore, during the FO process, the use of dispersed gels results in the formation of a viscous solution on the membrane rather than a wet solid. This feature can potentially reduce the viscosity of the draw agent on the membrane, thereby mitigating the internal concentration polarization effect [10]. Additionally, the dispersion of the draw agent in water enhances the contact between the draw agent and the membrane compared to using solid hydrogels. These attributes can lead to improved water flux in the FO process compared to experiments that use bulk gels with identical charge group content. Moreover, adjusting the morphology of hydrogels to achieve both high water flux and thermo-responsiveness is crucial. Another promising strategy involves incorporating light absorbers into the hydrogels [28]. These light absorbers can convert light into heat, thereby locally increasing the temperature of the hydrogels. This localized temperature increase allows for the

incorporation of a higher concentration of charged groups within the hydrogel network compared to hydrogels without light absorbers, even though a higher amount of charged groups typically raises the VPTT. Ideally, this temperature increase can be achieved through light radiation, such as natural sunlight. Carbon-based nanoparticles, like graphene oxide, which is well-known for their light-to-heat conversion capabilities [29], are among the materials utilized in various applications, including water desalination and purification [30–32]. Wang and coworkers were the pioneer in using carbon-based light absorbers in P (NiPAAm-*ran*-SA) hydrogels to increase the level of the water recovery of hydrogels. They showed that in hydrogels formed by random copolymerization of NiPAAm and SA, by using a high amount of carbon black as a light absorber, even almost 100 % water recovery is possible under radiation of UV light for 1 h. By decreasing the light absorber content, the water recovery decreases. They also showed that using reduced graphene oxide in such hydrogels has the same effect. One challenge for preparation of hydrogels containing nanomaterials is to stabilize them in the network structure of hydrogels. This concern is validate for nano-sized light absorbers like GO. One approach to achieve this stability is to introduce double bonds into the GO structure, enabling GO to participate in the polymerization reaction and chemically bond with the hydrogel network. Methacrylated GO, a modified form of GO with added double bonds, can be synthesized by reacting GO with 3-(trimethoxysilyl)propyl methacrylate. While hydrogels containing methacrylated GO have been studied in various applications, including biomedical fields, to the best of the author's knowledge, methacrylated GO has not yet been used as a light absorber within hydrogels for FO desalination applications.

In this study, P(NiPAAm-*ran*-SA) microgels with varying concentrations of charged groups are evaluated as draw agents for FO water desalination. These microgels are tested in both their dried form and as dispersions at concentrations of 40 wt% and 20 wt% in water. They are assessed against several feed solutions, including deionized (DI) water, a model brackish water solution with a concentration of 5 $g{\cdot}L^{-1}$, and a model seawater solution with a concentration of 35 $g{\cdot}L^{-1}$, providing an overall perspective on the potential of these microgels for FO water desalination. The FO experiments are conducted using two custom-made FO membranes with different water flux characteristics to emphasize the impact of membrane performance in conjunction with the draw agent. Additionally, some of the selected samples are synthesized with methacrylated graphene oxide to integrate a light absorber into the microgels. The results indicate that microgels with 25 mol% of charged comonomers, combined with modified graphene oxide in the network, offer the optimal balance between water flux and thermo-responsiveness.

2. Experiment

2.1. Materials

N-Isopropyl acrylamide (97 %), acrylic acid (97 %), *N*,*N*-methylenebisacrylamide, sodium hydroxide, ammonium persulfate, *m*-phenylenediamine, trimethylsilyl chloride, hexane, graphite flakes, sulfuric acid, phosphoric acid, 3-(trimethoxysilyl)propyl methacrylate, and a 25 wt% ammonia solution were sourced from Aldrich and used without additional purification. Poly(ether sulfone) (Ultrason 6020) was generously provided by BASF.

2.2. Synthesis of graphene oxide and methacrylated graphene oxide

Graphene oxide (GO) was synthesized following the procedure outlined by M. Tour and colleagues [33]. During each purification step, the product was precipitated by centrifugation at 10000 rpm for 1 h. The resulting GO is then reacted with 3-(trimethoxysilyl)propyl methacrylate to produce methacrylated graphene oxide (MeGO), which features double bonds on its surface.

To prepare MeGO, 0.1 g of GO was dispersed in 100 mL of water. The pH of this dispersion was adjusted to 10 using an ammonia solution. Subsequently, 5 mL of 3-(trimethoxysilyl)propyl methacrylate was added dropwise to the GO dispersion while the mixture was being sonicated. The reaction mixture was then heated at 50 °C overnight. Following the reaction, the mixture was undergone dialysis for 3 days against deionized (DI) water, with the water bath being replaced daily. The solution was then centrifuged at 10000 rpm for 1 h to separate the MeGO from the water. The resulting precipitated MeGO, with a concentration of 20 $mg{\cdot}mL^{-1}$ was stored in a refrigerator for future use.

2.3. Synthesis of microgels

P(NiPAAm-*ran*-SA) microgels with random copolymer molecular structure (Fig. 1C) were synthesized using a semi-batch, surfactant-free emulsion polymerization method [25,34]. To prepare these samples, a reactant mixture with a concentration of 0.07 $g{\cdot}mL^{-1}$ was slowly added to another reactant mixture with a concentration of 0.01 $g{\cdot}mL^{-1}$ at a temperature of 70 °C, where an initiator had already been added. For all samples, the cross-linking density was maintained at 0.7 mol%, based on the mole ratio of *N*,*N*-methylenebisacrylamide to the other monomers. The mole percentage of SA in the reaction mixture were set at 0, 8, 16, 25, and 50 %. These samples were designated as NiPSAX, where X represents the mole percentage of SA in the reaction mixture. For the synthesis of microgels containing GO, designated as NiPSAXGO, MeGO was used, which homogenously dispersed in the semi-batch solution at a concentration of 0.25 $mg{\cdot}mL^{-1}$.

As an example, to produce samples with 8 mol% SA, 26.1 mg of acrylic acid, 471 mg of NiPAAm, and 4.9 mg of *N*,*N*-methylenebisacrylamide were dissolved in 45 mL of water in a 250 mL three-necked flask. To this solution, 10.9 mg of sodium hydroxide dissolved in 5 mL of water was added dropwise. In a separate 100 mL flask, 182 mg of acrylic acid, 3.298 g of NiPAAm, and 34.2 mg of *N*,*N*-methylenebisacrylamide were dissolved in 42 mL of water, followed by the dropwise addition of 76 mg of sodium hydroxide dissolved in 5 mL of water. Both solutions were purged with nitrogen for 30 min. The three-necked flask is then placed in a 70 °C oil bath, and the solution from the second flask was transferred into a 60 mL syringe. After 15 min, 0.04 g of ammonium persulfate, dissolved in 3 mL of water, was added to the flask. The reaction mixture was stirred at 250 rpm using a magnetic stir bar. After approximately 20 min, the solution becomes slightly turbid. At this point, the second solution is injected at a rate of 3 $mL{\cdot}h^{-1}$ using a syringe pump (PHD Ultra, Harvard Apparatus). The reaction was allowed to continue overnight. Following this, heating was discontinued, and the mixture was stirred until it cools to room temperature. The solution was then transferred into dialysis tubes with a molecular weight cutoff of 6–8 kDa and placed in a 1.5 L water bath to remove unreacted substances and linear polymer chains. After three days of washing, the solution was dried either in an oven at 70 °C or by freeze-drying.

For the synthesis of microgels incorporating graphene oxide, a similar procedure was used, with 12.75 mg of MeGO dispersed in the semi-batch mixture.

The molar fraction of SA in the synthesized samples was assessed by the proton nuclear magnetic resonance spectroscopy (^{1}H NMR). ^{1}H NMR (400 MHz, D2O): δ 3.8 (1H, NHC$\underline{H}$), 1.2–2.2 (3H, C$\underline{H_2}$C$\underline{H}$ in polymer backbone), 1.05 (6H, NHCHC$_2\underline{H_6}$).

2.4. UV-spectroscopy

The VPTT of the microgels was determined using UV-spectroscopy by analyzing a 1 $mg{\cdot}mL^{-1}$dispersion of the samples in water. Transmission of UV light at a wavelength of 450 nm was measured using a JASCO V-600 UV-spectrometer over a period of 90 min. During this time, the temperature of the thermostat connected to the spectrometer was linearly increased from 15 °C to 60 °C. The temperature of the

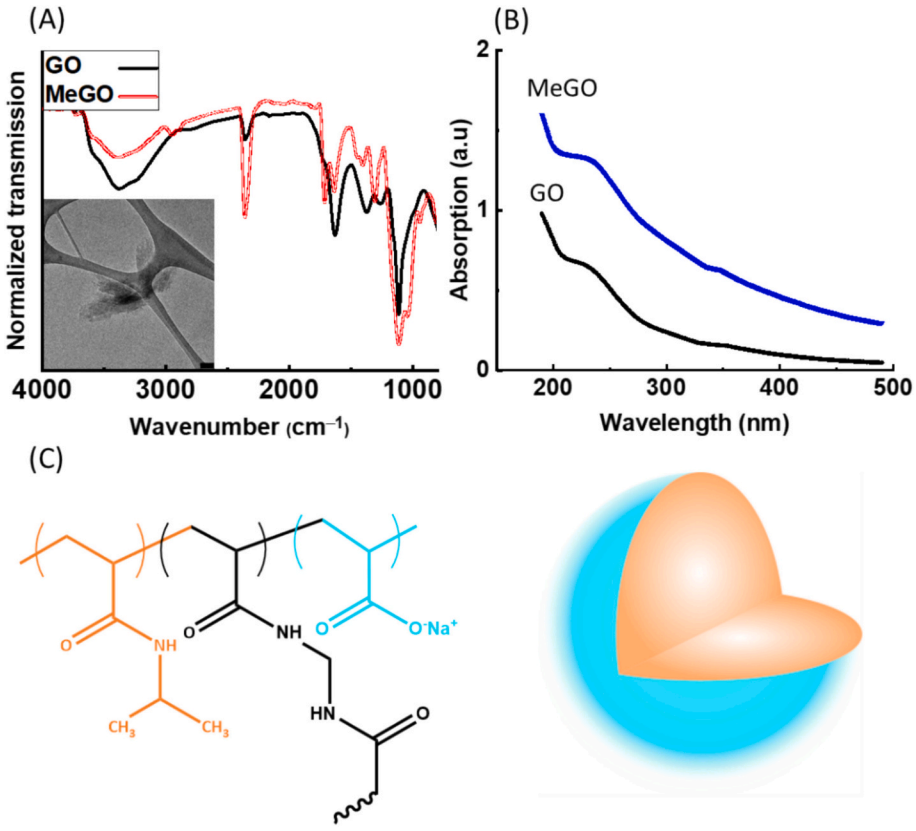

Fig. 1. (A) FTIR spectra of GO and MeGO, showing the characteristic functional groups and confirming the modification. The inset shows TEM image of lamellar GO. The scale bar depicts 100 nm, (B) UV–vis spectra of GO and MeGO, highlighting the light absorption properties. (C) Chemical structure of the random copolymer of NiPAAm (orange) and sodium acrylate (cyan) and the resulting core-shell microgel.

solution inside the UV cuvette was monitored to ensure that the temperature difference between the thermostat and the dispersion does not exceed 1 °C. The VPTT is calculated by analyzing the derivative of the transmission data as a function of temperature, which indicates the point at which the microgels undergo their volume phase transition [23].

To assess the thermo-responsivity of the microgel samples, UV–vis spectroscopy is employed, analyzing 1 mg·mL^{-1} aqueous dispersions between 15 °C and 60 °C. Above the VPTT, the samples exhibit turbidity and an opaque, milky appearance, which significantly alters the UV light transmission properties (see Fig. S1 in the supporting information). The VPTT is determined from the temperature at which the maximum change in transmission occurs, as calculated from the first derivative of the transmission-temperature data.

2.5. Transition electron microscopy

Transmission electron microscopy (TEM) was employed to visualize the synthesized microgels and to determine their average diameter. To prepare the samples, a 1 wt% dispersion of the microgels in water is made. Drops of this dispersion are then deposited onto copper grids supported with pure carbon (Ted Pella) or lacey carbon-covered copper grids (Ted Pella) and allowed to dry for 24 h. TEM bright field imaging was performed using a FEI Tecnai G2 Spirit TWIN LaB6 microscope operating at 120 kV. The imaging system was equipped with a TVIPS TemCam XF416 detector, which has a resolution of 4 K × 4 K pixels. This setup allows for high-resolution imaging of the microgels, facilitating accurate measurement of their size and morphology.

2.6. FO experiment

To assess the performance of the hydrogels as draw agents in FO, a custom-designed forward osmosis cell module was used, which is illustrated in Fig. S2. The setup included a membrane with a contact surface area of 4.9 cm^2, around which the feed solution circulates using a peristaltic pump. On the other side of the module, a cylindrical chamber with a diameter of 4.9 cm and a height of 5 cm was employed to hold either dried microgels or their aqueous dispersions. After equilibrating for 15 min, the weight of the feed solution is recorded at intervals of 5, 10, 15, 30, 45, and 60 min. The water flux (LMH) is calculated using the following formula:

$$J_w(\mathrm{LMH}) = \frac{\Delta m\ (\mathrm{g}) \times 10}{4.9(\mathrm{cm}^2)}$$

where: J_w is the water flux, Δm represents the change in the weight of the feed solution in grams (g) after 1 h of the experiment, and 4.9 cm^2 is the surface area of the membrane.

This method allowed for the evaluation of the hydrogels' effectiveness in drawing water through the semi-permeable membrane, providing insights into their performance as draw agents in the forward osmosis process. In addition to DI-water, a 5 g·L^{-1} model brackish water and 35 g·L^{-1} model seawater were tested as feed solutions. The model seawater was prepared by dissolving 24.53 g NaCl, 5.2 g $MgCl_2$, 4.09 g Na_2SO_4, and 1.16 g $CaCl_2$ in 1 L of water. The brackish water is obtained by diluting the seawater seven times.

The main membrane used in this work for FO experiment was a TFC membrane with Poly(ether sulfone) (PES) support layer coated with a poly(amide) (PA) active layer. The PES-PA membrane used was synthesized following a method, reported elesewhere [35]. A support layer was created via non-solvent phase inversion, using a casting solution of

PES, N-Methyl-2-pyrrolidone (solvent), and PEG-400 (pore-forming agent). The PA layer was then formed by interfacial polymerization of m-phenylenediamine (aqueous phase) and trimethylsilyl chloride (organic phase). SEM images of the support and PA layer morphology are now included in Fig. S3 of the supporting information. The support layer displays a finger-like pore structure, with a porosity of 75 % and a hydrophilicity contact angle of 72°. The PA layer has a ridge-and-valley morphology with an approximate thickness of 350 nm and a surface zeta potential of −15 mV at neutral pH.

2.7. Water recovery

To separate the water that transfers from the feed side to the draw side in the forward osmosis (FO) process and dilute the draw agent, the microgels must first be heated above their volume phase transition temperature (VPTT). Following this, the microgels should be separated from the released water through a filtration process, with the microgels dispersion acting as the feed. If the dispersed microgels are used as the draw agent, the separation of the diluted microgels dispersion from the water should continue until the concentration of the microgels dispersion returns to its initial value. To achieve this, the diluted draw agent was first irradiated with UV light at a power of 4 $kW{\cdot}m^{-2}$ for 30 min. The resulting mixture of shrunken microgels and water was then fed into a filtration cell designed to effectively remove the microgels from the dispersion. The setup involved circulating the feed dispersion around a membrane with a contact surface area of 4.9 cm^2. On the opposite side of the module, a small hole connected to a tube serves as the outlet for the permeate. A pressure pump facilitated the circulation of the feed dispersion into the filtration cell. This pump drew the dispersion through the filtration cell, where a portion of the feed permeates through the membrane and exits via the small hole as the filtrate. The remainder of the dispersion exited the cell and was returned to the original container of the feed solution. Along the return flow path, a pressure gauge and a valve were installed to monitor and control the pressure within the system. This setup allowed for effective separation of the microgels from the water, ensuring that the microgels are retained while the water was recovered and separated.

3. Results and discussion

3.1. Synthesis of GO, MeGO, and microgels

The characterization of synthesized GO by Fourier-transform infrared spectroscopy (FTIR) confirm the successful synthesis of GO, as the FTIR spectrum shown in Fig. 1A displays characteristic peaks: O—H stretching vibrations at 3380 cm^{-1}, C═C stretching from unoxidized aromatic SP^2 CC bonds at 1620 cm^{-1}, C-OH bending at 1375 cm^{-1}, epoxy C—O stretching at 1250 cm^{-1}, and alkoxy C—O stretching at 1120 cm^{-1}. Transmission electron microscopy (TEM) images of GO reveal a lamellar layer structure with an approximate size of 1 μm. The UV–vis spectrum of GO, depicted in Fig. 1B, shows an absorbance peak at 232 nm, which corresponds to the $\pi \rightarrow \pi^*$ transition of the C—C conjugated aromatic domains. MeGO is synthesized by reacting GO with 3-(trimethoxysilyl)propyl methacrylate in a basic aqueous medium. The FTIR spectrum of MeGO, also shown in Fig. 1A, indicates a reduced peak area for the O—H stretching vibrations compared to GO. This decrease is due to the reaction between the hydroxyl groups on GO and the trimethoxysilyl group. Additional peaks observed at 2951 cm^{-1} (C—H bond vibration), 1710 cm^{-1} (C═O bond vibration), 1307 cm^{-1} (Si—C bond vibration), and 1116 cm^{-1} (Si—O bond vibration) confirm the successful formation of MeGO. The absorbance wavelength of MeGO is similar to that of GO, indicating that the methacrylation did not significantly alter the optical properties of the graphene oxide.

The synthesized microgels consist of random copolymer chains of NiPAAm and SA, interconnected by methylene bisacrylamide units (Fig. 1C). Since PNiPAAm has an LCST characteristic, NiPAAm units become hydrophobic at the polymerization temperature of 70 °C, phase-separating from water and forming aggregates, while SA units remain dispersed, resulting in a core-shell structure [25,34]. In case of using MeGo, this nanosized light absorbers is chemically incorporated into the microgel network through the reaction of the unsaturated C═C bonds of the methacrylate units on the surface of MeGO with the growing network strands during the microgels formation.

The nuclear magnetic resonance (NMR) spectra of synthesized microgels, shown in Fig. S4 in the supporting information, allowed for determining the ratio of SA to NiPAAm by comparing the chemical shifts at $\delta = 3.8$ ppm (CH of NiPAAm units) and $\delta = 1.2–2.2$ ppm (CH and CH2 in the backbone of the network strands). The results are summarized in Table 1. For samples with relatively low SA content, the ratio of SA to NiPAAm in the microgels closely matches that of the reaction mixture. However, as the SA/NiPAAm ratio increases, a greater discrepancy between the reaction mixture ratio and the synthesized microgels is observed.

In emulsion polymerization, polymers typically form round particles, which are visualized using TEM. TEM images of the microgels shown in Figs. 2 and S5 revealed that increasing the SA content reduced the average particle size from 1.51 μm to less than 77 nm. This reduction can be attributed to the repulsive effects of SA units, which act similarly to surfactants by stabilizing individual particles and preventing their agglomeration [27]. Furthermore, a higher SA content results in reduced aggregation of NiPAAm units during polymerization, thereby leading to smaller particle sizes. This phenomenon is further discussed in the subsequent section. For sample NiPSA25GO, three average microgel sizes are observed: 160 nm, 486 nm, and 1.62 μm. This size diversity is attributed to the effect of MeGO and its hydrophobic modified surface on the aggregation of PNiPAAm. Since MeGO was dispersed in the semi-batch solution, its concentration in the reaction flask increased from 0 (at time 0) to 0.12 $mg{\cdot}mL^{-1}$ by the end of the injection process. Thus, the concentration of MeGO varied continuously during the reaction. In microgels with a higher MeGO content, stronger aggregation occurs, and the surfactant effect of SA becomes weaker, resulting in larger particles similar in size to NiPSA0. Conversely, when the MeGO content is lower, aggregation is weaker, and the surfactant effect of SA predominates, leading to smaller microgels. This variability in MeGO content within the microgels is likely due to the dispersion of MeGO in the semi-batch reactant mixture, resulting in an inconsistent concentration during the reaction. We avoid dispersing MeGO in the batch mixture to prevent it from being exposed to 70 °C for the entire reaction duration, which could destabilize its dispersion in water.

3.2. Thermo-responsivity of microgels

Linear PNiPAAm typically exhibit a lower critical solution temperature (LCST) around 32 °C, which marks a transition in water solubility. This behavior is linked to the aggregation of the nonpolar parts of NiPAAm units when the temperature exceeds this threshold [36,37]. Above the LCST, these aggregates overshadow the hydrophilic segments, rendering NiPAAm a hydrophobic material. Consequently, the network formed by NiPAAm exhibits a distinct transition temperature.

Table 1
Summary of the physical and chemical properties of the synthesized microgels, including their composition, average particle size, and volume phase transition temperature (VPTT).

Sample	SA/NiPAAm in feed solution	SA/NiPAAm in product	Average diameter (nm)	VPTT (°C)
NiPSA0	0	0	1510±30	31.98
NiPSA8	0.08	0.09	502±89	48.83
NiPSA16	0.16	0.16	443±34	52.43
NiPSA25	0.25	0.30	216 ±29	–
NiPSA25GO	0.25	0.35	160±27/1616±110	41.09
NiPSA50	0.50	0.61	112±21	–

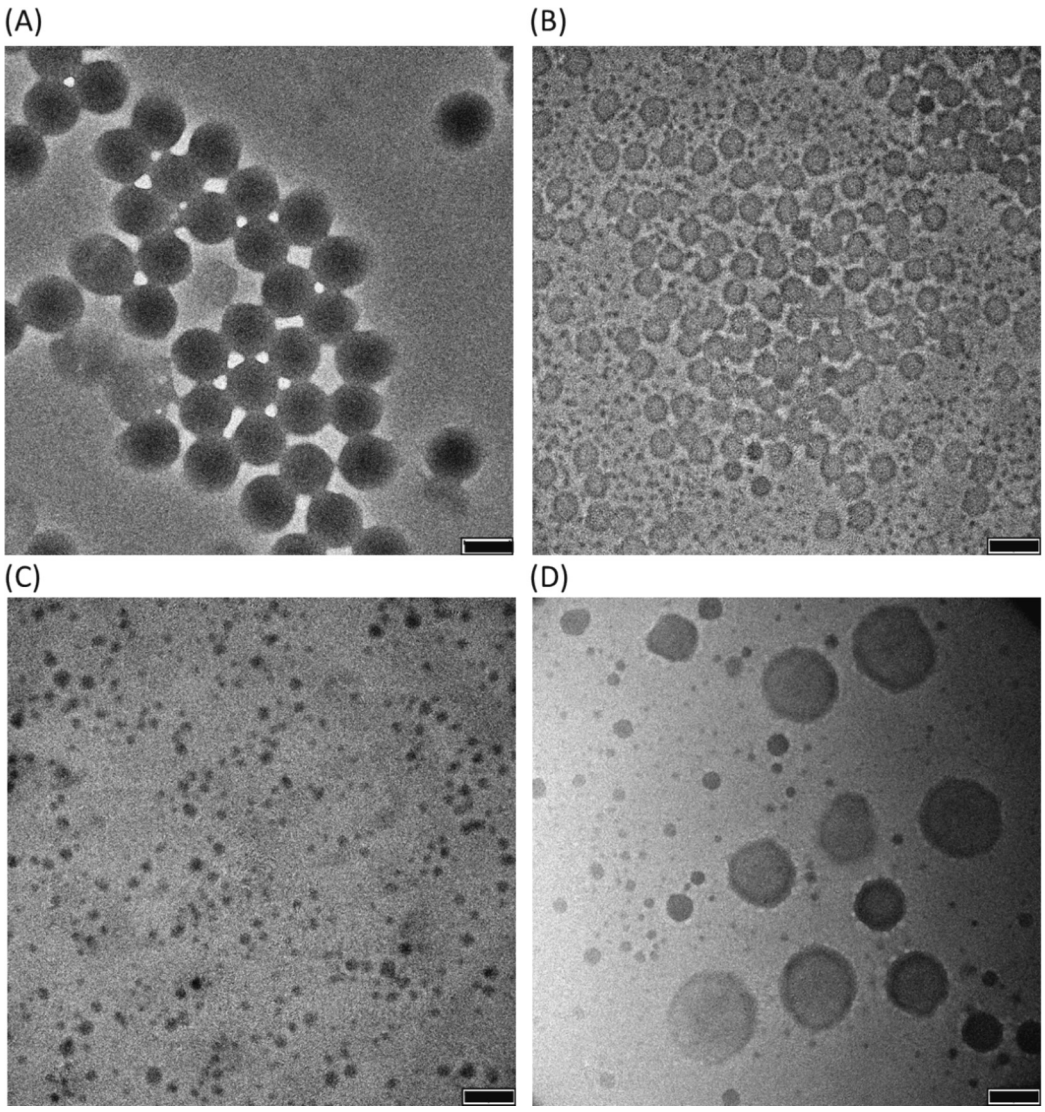

Fig. 2. TEM images of microgels samples: (A) NiPSA0, (B) NiPSA16, (C) NiPSA25, and (D) NiPSA25GO illustrating their morphological differences. The scale bars depicts 1 μm.

Below this temperature, the network remains hydrophilic and swells in water, whereas above the transition temperature, it becomes hydrophobic, leading to a significant reduction in its water retention capacity. As a result, NiPAAm gels shrink when heated above the transition temperature, releasing a portion of the water absorbed at lower temperatures. The VPTT of NiPAAm copolymers is influenced by the hydrophilicity of the comonomer units and their proportion within the copolymeric network. Our previous studies on bulk gel samples demonstrated that increasing the content of ionic units raises the VPTT of the NiPAAm copolymeric network [23,38]. This shift occurs because a higher concentration of ionic units necessitates greater aggregation to overpower the hydrophilic components, which typically occurs at elevated temperatures.

Above the VPTT, the samples exhibit turbidity and an opaque, milky appearance, which significantly alters the UV light transmission properties (see Fig. S1 in the supporting information). The results of the transmission of UV light from samples as a function of temperature are illustrated in Fig. 3A. The VPTT values for samples NiPSA0, NiPSA8, and NiPSA16 are found to be 31.98 °C, 48.83 °C, and 52.43 °C, respectively, as indicated by the minima in the first derivative of the transmission data with respect to temperature as illustrated in Fig. 3B. Notably, the samples containing 25 and 50 mol% SA comonomers do not exhibit any change in UV light transmission up to 60 °C. This lack of change suggests that these samples do not reach a clear transition within the studied temperature range. Although UV light transmission of 1 $mg{\cdot}mL^{-1}$ dispersions of NiPSA25 and NiPSA50 does not show significant changes up to 60 °C (and even 70 °C), the NiPSA25 reaction mixture becomes turbid during polymerization at 70 °C. This indicates that NiPAAm units aggregate even with 25 mol% SA, but the aggregation level is insufficient to induce turbidity in low concentration (1 $mg{\cdot}mL^{-1}$) dispersions. Further investigation with UV-spectroscopy on NiPSA25 dispersions at concentrations ranging from 1 $mg{\cdot}mL^{-1}$ to 40 $mg{\cdot}mL^{-1}$ (Fig. 3C) reveals that turbidity develops in the temperature range of 20–60 °C when the concentration exceeds 4 $mg{\cdot}mL^{-1}$. This phenomenon is not observed for NiPSA50, even at the highest studied concentration, suggesting that higher SA content leads to a more stable dispersion with less pronounced turbidity under similar conditions. In short, increasing SA content raises the VPTT, while the extent of this shift, as measured by UV–vis, depends on the microgel concentration.

Interestingly, for samples NiPSA8 and NiPSA16, the first derivative of the transmission data reveals a shoulder or a distinct second peak at temperatures lower than the primary peak. This indicates that the NiPAAm and SA units in these microgels are not homogeneously distributed. Instead, there appear to be at least two distinct phases

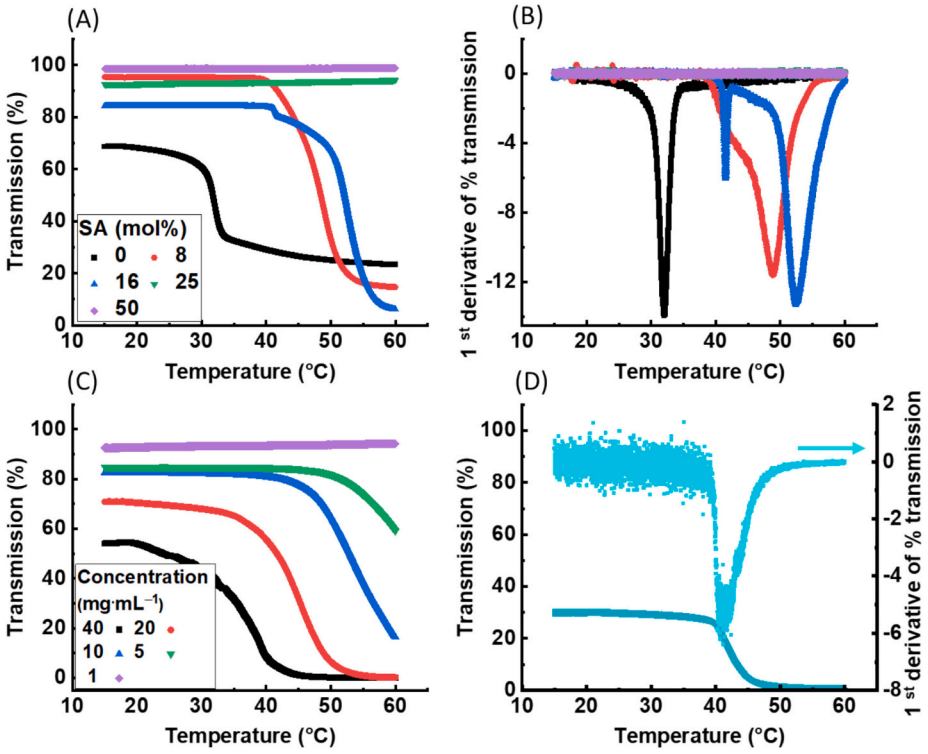

Fig. 3. (A) UV–vis spectra of microgels with varying SA content at 1 mg·mL^{-1}. (B) first derivative of data of part A. (C) spectra of NiPSA25 at different concentration. (D) Spectra of NiPSA25GO at 1 mg·mL^{-1}.

within the particles: one phase rich in NiPAAm, exhibiting a lower VPTT, and another phase with a lower NiPAAm content, which has a higher VPTT. This multi-phase structure resembles a core-shell morphology, where the core is primarily composed of NiPAAm, while the outer layers are enriched with SA. During emulsion polymerization at 70 °C, it is likely that a phase with a high SA content forms the surface area of the particles, which does not transition below 60 °C and thus remains undetectable by UV–vis spectroscopy.

The thermo-responsivity of sample with 25 mol% of SA in the reaction mixture incorporating MeGO in the semi-batch solution (NiPSA25GO) is also assessed using UV–vis spectroscopy. The results is presented in Fig. 3D. Contrary to the observations for samples without GO, the transmission of NiPSA25GO at concentration of 1 mg·mL^{-1} decreases with increasing temperature. This result suggests that the VPTT of NiPSA25GO is approximately 41 °C. This notable shift in the phase diagram of the microgels is likely attributable to the incorporation of MeGO. It is well established that the copolymerization of NiPAAm with 3-(trimethoxysilyl)propyl methacrylate tends to lower the VPTT due to the hydrophobic nature of the methacrylate units [39]. This effect occurs because methacrylate units, being hydrophobic, reduce the overall hydrophilicity of the polymer network, thereby lowering the temperature at which the transition from hydrophilic to hydrophobic states occurs. In the case of NiPSA25GO, the presence of methacrylate units from MeGO in the reaction mixture likely counteracts, to some extent, the increase in VPTT caused by the SA units. As a result, the methacrylate units from MeGO become integrated into the microgel network, contributing to the observed decrease in transition temperature.

3.3. Light-responsivity of microgels

To assess the impact of GO on UV-light absorption and its subsequent conversion to heat, dispersions of GO in water at concentrations of 1 and 3 mg·mL^{-1} are subjected to UV irradiation. The UV-light power used is 4 kW·m^{-2}, and the temperature of the dispersion is monitored with a digital thermometer. The results, shown in Fig. S6 of the Supporting Information, indicate that the temperature increase (ΔT) for these solutions is 9.9 ± 0.66 °C and 10.66 ± 0.38 °C, respectively. In contrast, DI-water under similar conditions showed a temperature rise of only 4.3 ± 0.32 °C. These results underscore the effectiveness of GO in absorbing UV-light and converting it to heat. A comparative study is also conducted on microgel dispersions with concentrations of 1 wt% and 4 wt%. The temperature increases for these microgel dispersions were 5.56 ± 0.57 °C and 5.76 ± 0.26 °C, respectively. Compared to DI-water, the temperature rise due to microgels is relatively modest, suggesting that microgels alone have a limited capacity for UV-induced heating. In stark contrast, microgel samples containing MeGO exhibit a significantly different behavior. For a 1 wt% dispersion of NiPSA25GO, the temperature increase is 10.26 ± 1.02 °C, and for a 4 wt% dispersion, it is 11.40 ± 0.82 °C. When the radiation time is extended to 15 min, the temperature of NiPSA25GO rose by 20 °C. Additionally, an experiment conducted under natural sunlight on a sunny day in Mainz city (ambient temperature of 33 °C) showed that after 30 min, the temperature of NiPSA25GO reached 40.4 ± 0.21 °C, with the sample displaying partial turbidity. These findings highlight the superior performance of MeGO-enhanced microgels in converting UV-light to heat compared to microgel samples without GO. The increased temperature response observed in the MeGO-containing microgels indicates their potential for applications requiring light-responsive heating.

3.4. Forward osmosis water desalination

Before evaluating hydrogels in the FO experiment, it is necessary to assess the performance of the flat sheet, thin-film composite membrane utilized in this work. In a reference FO test, with DI-water as the feed solution and 1 M NaCl as the draw solution, when the membrane's active layer is oriented towards the feed solution (Active Layer Facing the Feed Solution, ALFS, or FO mode), the membrane exhibited a water flux of 12 L·m^{-2}·h^{-1} (LMH), a reverse salt flux of 2.44 g·m^{-2}·h^{-1} (gMH), and selectivity of 0.2 g·L^{-1}. The water flux reaches 20 LMH when the

membrane's active layer faces the 1 M NaCl draw solution (Active Layer Facing the Draw Solution, ALDS, or PRO mode). For experiments with microgels as draw agents, however, the Active Layer Facing the Feed Solution (ALFS) configuration is used to prevent potential damage to the membrane's top active layer from the gels. Before each experiment, the system is allowed to equilibrate for at least 15 min to ensure the absence of residual water in the module or from the membrane. Subsequently, either 0.2 g of dried microgels or 4 g of microgel dispersion at 20 wt% or 40 wt% concentration is placed on top of the membrane.

The performance of dried microgels as draw agents is first evaluated across three feed solutions: DI-water, 5 g·L^{-1} brackish water, and 35 g·L^{-1} seawater. The results of the water flux measurements are summarized in Fig. 4A. As expected for a FO process, water flux decreases as the salt concentration in the feed solution increases. This reduction is attributed to the diminishing difference in osmotic pressure between the microgels and the feed solution. Higher salt concentrations in the feed solution reduce the driving force for water movement through the membrane. For each feed solution, water flux generally increases with the addition of more SA, charged groups in the microgels. This is because the increased osmotic pressure resulting from a higher content of charged groups enhances the driving force for water transport. This trend is more pronounced when using DI-water as the feed solution. As the salt concentration in the feed solution rises (brackish and seawater), the impact of increased charged groups on water flux becomes less noticeable. These observations suggest that while the presence of charged groups improves water flux, the benefit is more significant in lower salinity environments where the osmotic pressure difference between the draw agent and the feed solution is greater. Furthermore, in this study, the increase in water flux resulting from the higher SA content can also be attributed to the reduction in particle size. Smaller particles have a larger surface area, which enhances the contact between the microgels and membranes when they are dried.

The water flux in a FO process is particularly affected by the internal concentration polarization, which is sensitive to the viscosity (diffusivity) of the draw agent [10]. When microgels are used in their dried state, internal concentration polarization effects are at their most critical. The high viscosity of the dried microgels maximizes internal concentration polarization, which impairs the overall efficiency of the FO process. Additionally, the contact between the dried draw agent and the membrane is suboptimal. To address these issues, the performance of microgels in their dispersed state is evaluated. Two dispersion concentrations are tested: 40 wt% and 20 wt%. Regarding these high concentrations, it is noted that while dispersing microgels in water decreases the viscosity of dispersion, dispersed microgels at low concentrations are less effective due to the low osmotic pressure. Therefore, a balance is necessary to optimize performance. Samples NiPSA16 and NiPSA25 are chosen for evaluation in their dispersed state due to their balance between water flux and thermo-responsivity. Sample NiPSA50, although having higher water flux compared to NiPSA16 and NiPSA25, lacks thermo-responsivity below 60 °C, making it less suitable for this test. As illustrated in Fig. 4B and C, a 40 wt% dispersion of NiPSA16 is unable to draw 35 g/L of seawater. Similarly, neither sample can extract 35 g/L of seawater using a 20 wt% dispersion. Notably, both NiPSA16 and NiPSA25 exhibit higher water flux at the 40 wt% concentration compared to the 20 wt% concentration. In fact, both NiPSA16 and NiPSA25 in 20 wt% dispersions demonstrate lower effectiveness. The lower osmotic pressure at this concentration results in insufficient driving force for effective water flux. Furthermore, NiPSA25 outperforms NiPSA16 by more effectively drawing feed solutions. In addition to the impact of a higher number of charged groups in NiPSA25, the increased water flux observed for this sample compared to NiPSA16 can also be attributed to its lower viscosity. This reduced viscosity may improve water flux by mitigating internal concentration polarization effects and enhancing interaction with the membrane, as indicated by the viscosity data presented in Fig. S7 (Supporting Information).

To further analyze the impact of microgel concentration on water flux, the data are replotted in Fig. 5A and B. In these figures, the water flux for dried microgels, as well as for 20 wt% and 40 wt% dispersions, is compared across different feed solutions. For NiPSA16, the water flux decreases when microgels are dispersed, regardless of the feed solution used. For NiPSA25, dispersing microgels at a concentration of 40 wt% results in an increased water flux when tested against DI-water. This improvement is also observed, albeit less significantly, for the 5 g·L^{-1} brackish water feed solution. However, for the 35 g·L^{-1} seawater feed solution, the water flux of dried NiPSA25 and its 40 wt% dispersion are nearly identical. Reducing the concentration to 20 wt% for NiPSA25 leads to decreased water flux across all feed solutions compared to the 40 wt% dispersion. The lack of a distinct trend regarding the effect of microgel concentration on water flux can be attributed to the interplay of two factors: the reduction of osmotic pressure when microgels are dispersed in water, which generally decreases water flux, and the reduction in viscosity of the draw agent, which can mitigate internal concentration polarization effects as well as improvement of the water flux due to better contact between the draw agent and the membrane. In conclusion, the relationship between microgel concentration and water flux is complex, influenced by the balance between osmotic pressure and viscosity. The results underscore the importance of optimizing these factors to enhance performance in forward osmosis processes.

To examine the effect of membrane characteristics on microgels performance [40], NiPSA25 at different concentrations is tested against 5 g·L^{-1} brackish water and 35 g·L^{-1} seawater using a membrane with a significantly improved water flux of 22 LMH [41]. This flux is approximately twice the water flux achievable with our PES-PA thin film composite membrane. The results, presented in Fig. 6, show a considerable enhancement in water flux with the new high-performance membrane. Specifically, the flux for 5 g·L^{-1} brackish water ranged from 2.84 to 4.79 LMH, whereas for 35 g·L^{-1} seawater, it ranged from 0.81 to 1.36 LMH. This improvement is attributed to the membrane

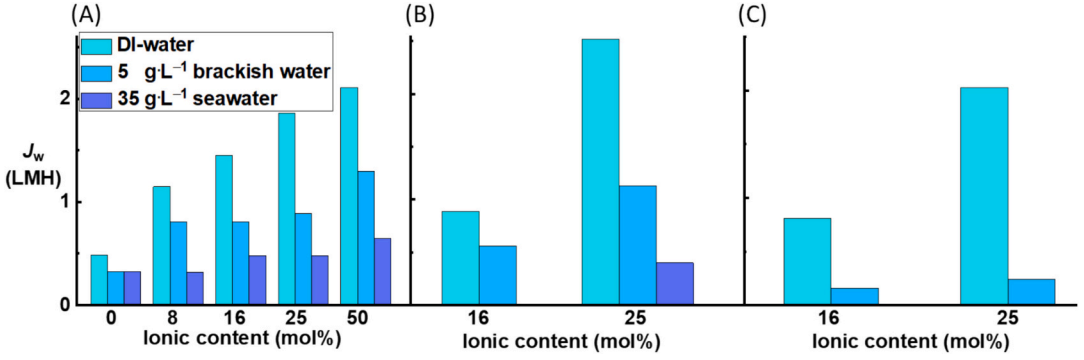

Fig. 4. Water flux generated by microgels with varying SA content in forward osmosis experiments using DI water, 5 g·L^{-1} brackish water, and 35 g·L^{-1} seawater. (A) Dried samples, (B) 40 wt% dispersion, and (C) 20 wt% dispersion.

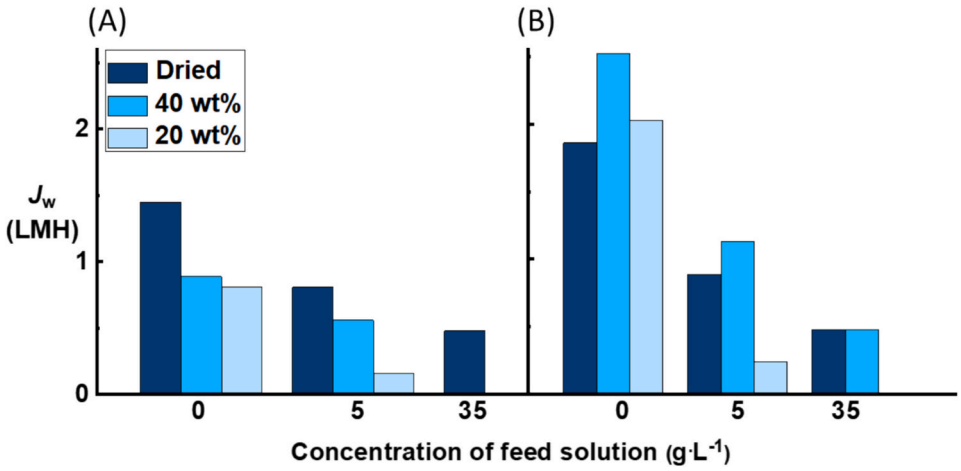

Fig. 5. Water flux generated by microgels with (A) 16 mol% SA and (B) 25 mol% SA in forward osmosis experiments using DI water, 5 g·L^{-1} brackish water, and 35 g·L^{-1} seawater at three states: dried, 40 wt% dispersion, and 20 wt% dispersion.

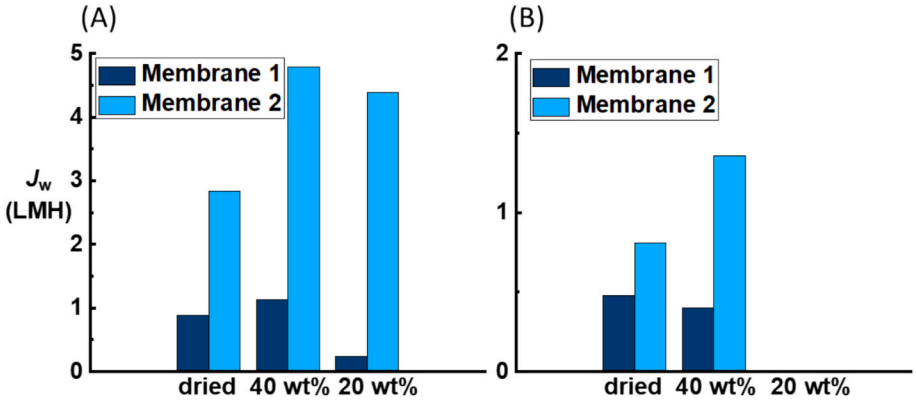

Fig. 6. Comparison of the performance of NiPSA25 in forward osmosis experiments using two different types of membranes. (A) 5 g·L^{-1} brackish water as the feed solution, (B) 35 g·L^{-1} seawater as the feed solution.

structure, which features a microfiltration membrane. This membrane has an average pore size of 100 nm. SEM images confirm this average size but also show some larger pores up to 1 μm and a higher porosity than the PES-PA membrane (see Fig. S8 in the supporting information). The large pore size of this support not only enhances water transport but also reduces the internal concentration polarization effect via diffusion of microgels into pores of support layer. In this regard, the flexibility of hydrogels in their hydrated state should be considered. Notably, with this membrane, the 40 wt% dispersion shows a significant enhancement of flux compared to the dried sample, a difference that was not as apparent in experiments using the lower performance membrane. However, it should be considered that even with this membrane, the 20 wt% dispersion of NiPSA25 is still unable to draw 35 g·L^{-1} seawater due to insufficient osmotic pressure difference, and the use of a higher-performance membrane does not change this result. It should be noted that in all FO experiments the water fluxes of NiPSA25GO are nearly identical to those of NiPSA25. For comparison, the water flux achieved with microgels can be evaluated against standard draw solutions, such as NaCl solution. Using Membrane 1 and Membrane 2, a 1 M NaCl solution draws DI water with water fluxes of 12 and 22 LMH, respectively. When the feed solution is switched to seawater, these fluxes decrease to 3.70 and 6.78 LMH. Additionally, for both membranes, replacing NaCl solution with $MgCl_2$ solution is expected to reduce water flux by approximately 40 % [10].

3.5. *Water recovery*

Water recovery is not only crucial for the separation of absorbed water from microgels but also for the potential reuse of microgels as draw agents in desalination processes. For bulk thermo-responsive hydrogels, the typical methods for water recovery involve either heating the hydrogels above their VPTT or employing a combination of heating and pressure. In this study, when the samples are heated above their VPTT, they exhibited increased turbidity due to the aggregation of NiPAAm-enriched regions within the microgels. Despite this turbidity, the aggregates did not undergo macroscopic phase separation from the water in a manner that could be easily filtered using standard filter papers of grades 1–4. This phase separation only occurred partially for relatively large microgels when the concentration of the dispersion is above 10 wt%. For achieving further separation of microgels and water, membranes with smaller pore sizes are required. Typically, applying pressure is necessary for such filtration processes. To explore this, a filtration setup is designed as described in the Experimental section and illustrated in Fig. S9 in the supporting information, in which a commercial microfiltration membrane is employed. This pore size is deemed suitable for samples NiPSA16 and NiPSA25, considering their average diameters measured by TEM. Separation of water and microgels by this setup is investigated for samples NiPSA16, NiPSA25, and NiPSA25GO. The 5 mg·mL^{-1} dispersion of these samples is initially heated above their volume phase transition temperature (VPTT). These turbid dispersions are then utilized as the feed solution in the filtration setup. For all three

samples, the concentration of microgels in the permeate solution is negligible, indicating that the membranes effectively rejected nearly 100 % of the microgels, allowing only the water to pass through. This shows that although the employed membrane has relatively large pore size, it is still small enough that does not allow microgels to permeate through.

In a more practical scenario, as illustrated in Scheme 1, a 20 wt% dispersion of NiPSA25GO is utilized as the draw agent to desalinate 5 g·L^{-1} brackish water. After one hour of the FO experiment, the concentration of the microgels decreased to 12 wt% due to the water transport from the feed side to the draw agent side. This reduced dispersion can reach its VPTT when exposed to UV light or natural sunlight. Under these conditions, the microgels shrink and release the absorbed water, which can then be separated using the filtration setup. The shrinkage and subsequent aggregation of the microgels result in a milky or turbid dispersion. This milky/turbid dispersion is used as the feed for the filtration process. During the filtration process, the microgels are retained by the membrane and returned to the feed container, while the purified water permeated through the membrane with a flux of 36 LMH. The filtration process is halted when the concentration of the feed solution reached 20 wt%. This solution could then be reused as a draw agent for desalinating brackish water. Two points are essential for the filtration process. First, during filtration, the feed solution should appear milky or turbid, indicating microgels shrinkage. To maintain turbidity, the process should either be conducted quickly to prevent feed cooling or performed under continuous UV or sunlight radiation. In our tests, the process was fast enough to maintain turbidity without continuous irradiation. Second, this process is repeatable multiple times without significant performance loss. For sample NiPSA25GO, water-drawing efficiency decreased by less than 10 % after five FO-water recovery cycles, with no notable reduction in responsiveness.

4. Conclusion

Thermo-responsive microgels studied in this work exhibit substantial potential as draw agents in FO process for the desalination of brackish or seawater. The ability to use these microgels in a dispersed state, rather than a dried state, provides a significant advantage by reducing the internal concentration polarization effect and improving contact with the membrane surface. Additionally, it is potentially feasible to circulate microgel dispersions in a cross-flow FO setup. Incorporating MeGO into the microgels offers the added benefit of light absorption and subsequent conversion to heat, raising the temperature of the microgel dispersion. In general, increasing SA content enhances water flux while diminishing thermo-responsivity. Among the studied samples, microgels with 25 mol % SA in the reaction mixture (30 mol% SA in microgels) containing MeGO represent a balance between water flux in FO experiments and thermo-responsivity. Using a high-performance membrane, dried samples, and 40 wt% and 20 wt% dispersions draw 5 g·L^{-1} brackish water with water fluxes of 2.84, 4.79, and 4.39 LMH, respectively. The values for 35 g·L^{-1} seawater are 0.81, 1.36, and 0 LMH, respectively. The VPTT of this sample is 41 °C. Notably, through the combined effects of light absorption and heat generation, this temperature can be reached under natural conditions on a 33 °C day within just 15 min or by using artificial UV light radiation at room temperature. Under these conditions, the diluted draw agent can then be recovered to its original concentration using a microfiltration membrane under 2–4 bar of pressure, achieving a permeate flux of 36 LMH. This study proposes an efficient two-step desalination process: water drawing using thermo-responsive microgels dispersed in water as draw agents, followed by water recovery through microfiltration under 2–4 bar pressure. This process could be further improved by implementing a continuous setup for the first step.

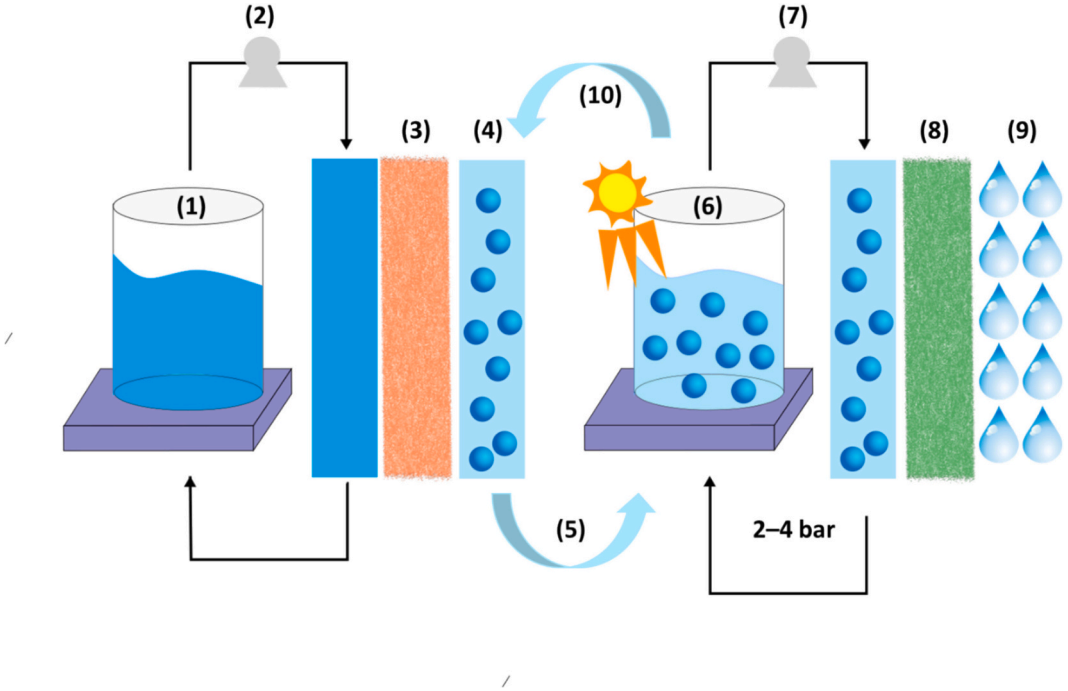

Scheme 1. Illustration of desalination process in this work: The process begins with the feed solution (e.g., 5 g·L^{-1} brackish water) (1) being circulated using a peristaltic pump (2) through a semi-permeable FO membrane (3). Water-dispersed microgels (e.g., 20 wt%) (4) draws water from the feed solution. After FO, the diluted microgels dispersion (e.g., 12 wt%) is transferred to the microfiltration process (5). During microfiltration, the feed dispersion (6) is irradiated with natural sunlight or UV radiation (or a combination of heating and radiation) to reach its volume phase transition temperature. The dispersion is circulated using a pressure pump (7) that generates 2–4 bar pressure. A microfiltration membrane (8) with appropriate pore size allows water to pass through but retains the microgels, producing purified water as permeate (9). The concentrated microgels dispersion is then reused as the draw agent in the FO process (10).

CRediT authorship contribution statement

Amir Jangizehi: Conceptualization, Methodology, Investigation, Writing – review & editing, Supervision. **Jan Eckhardt:** Investigation. **Karolina Izabela Borkowska:** Investigation. **Zsolt Dallos:** Investigation. **Melanie Bauer:** Investigation. **Hasan Salehi:** Investigation. **Reza Razavi:** Investigation. **Alireza Shakeri:** Formal analysis. **Seyed Abdollatif Hashemifard:** Formal analysis. **Sebastian Seiffert:** Conceptualization, Supervision, Funding acquisition.

Declaration of competing interest

The authors declare that they have no known competing financial interests or personal relationships that could have appeared to influence the work reported in this paper.

Acknowledgement

This research was funded by the German Federal Ministry of Education and Research (BMBF) in the framework of the MEWAC program under the HydroDeSal project (Project Code 02WME1613). PD Dr. Ute Kolb from the University of Mainz and the Technical University of Darmstadt is acknowledged for her assistance with TEM measurements. Dr. Erik Gubbels from BASF is also gratefully thanked for supplying the Poly(ether sulfone) (Ultrason 6020). We gratefully acknowledge the HydroDeSal project partners for their scientific collaboration: Prof. Michael Maskos, Christoph Bantz, Conrad Nickel, and Martin Berger (Johannes Gutenberg University of Mainz), as well as Prof. Qusay F. Alsalhy and Dhiyaa Al-Timimi (University of Technology-Iraq).

Appendix A. Supplementary data

Supplementary data to this article can be found online at https://doi.org/10.1016/j.desal.2024.118314.

Data availability

Data will be made available on request.

References

[1] Water Scarcity in the Middle East Hub, N., NATO, Italy, (2019).
[2] A. Cipollina, G. Micale, L. Rizzuti, Con-Ventiona L and Renewable Energy Processes, Springer-Verlag, Berlin & Heidelberg, 2009.
[3] M. Elimelech, W.A. Phillip, Science 333 (2011) 712–717.
[4] G. Amy, N. Ghaffour, Z. Li, L. Francis, R.V. Linares, T. Missimer, S. Lattemann, Desalination 401 (2017) 16–21.
[5] S.K. Patel, P.M. Biesheuvel, M. Elimelech, Acs Es&T Engineering 1 (2021) 851–864.
[6] M. Qasim, M. Badrelzaman, N.N. Darwish, N.A. Darwish, N. Hilal, Desalination 459 (2019) 59–104.
[7] L. Francis, O. Ogunbiyi, J. Saththasivam, J. Lawler, Z. Liu, Environ. Sci.: Water Res. Technol. 6 (2020) 1986–2015.
[8] M. Mohammadifakhr, J. de Grooth, H.D. Roesink, A.J. Kemperman, Processes 8 (2020) 404.
[9] N. A. Thompson, and P. G. Nicoll, Forward osmosis desalination: A commercial reality. In *IDA World Congress–Perth Convention and Exhibition Centre (PCEC),* Perth, Western Australia September, (2011), pp. 4–9.
[10] D.L. Shaffer, J.R. Werber, H. Jaramillo, S. Lin, M. Elimelech, Desalination 356 (2015) 271–284.
[11] W. Suwaileh, N. Pathak, H. Shon, N. Hilal, Desalination 485 (2020) 114455.
[12] Y. Cai, Desalination 391 (2016) 16–29.
[13] J. Wang, S. Gao, J. Tian, F. Cui, W. Shi, Water 12 (2020) 692.
[14] J. Zeng, S. Cui, Q. Wang, R. Chen, Desalination 459 (2019) 105–113.
[15] K. Zhang, F. Li, Y. Wu, L. Feng, L. Zhang, Desalination 495 (2020) 114667.
[16] H. Cui, H. Zhang, M. Yu, F. Yang, Desalination 426 (2018) 118–126.
[17] O. Okay, In *Hydrogel Sensors and Actuators*, Springer, Heidelberg, 2009, pp. 1–14.
[18] K. Varaprasad, G.M. Raghavendra, T. Jayaramudu, M.M. Yallapu, R. Sadiku, Mater. Sci. Eng. C 79 (2017) 958–971.
[19] D. Li, X. Zhang, J. Yao, G.P. Simon, H. Wang, Chem. Commun. 47 (2011) 1710–1712.
[20] H. Feil, Y.H. Bae, J. Feijen, S.W. Kim, Macromolecules 26 (1993) 2496–2500.
[21] Y. Liu, J.L. Velada, M.B. Huglin, Polymer 40 (1999) 4299–4306.
[22] S. Hirotsu, Y. Hirokawa, T. Tanaka, J. Chem. Phys. 87 (1987) 1392–1395.
[23] A. Jangizehi, S. Seiffert, J. Chem. Phys. 154 (2021) 144902.
[24] Y. Cai, W. Shen, S.L. Loo, W.B. Krantz, R. Wang, A.G. Fane, X. Hu, Water Res. 47 (2013) 3773–3781.
[25] Y. Hartanto, S. Yun, B. Jin, S. Dai, Water Res. 70 (2015) 385–393.
[26] C.L. Lin, W.Y. Chiu, C.F. Lee, J. Polym. Sci. Part A. Polym. Chem. 44 (2006) 356–370.
[27] Q. Zhang, L. Zha, J. Ma, B. Liang, J. Colloid Interface Sci. 330 (2009) 330–336.
[28] D. Li, X. Zhang, J. Yao, Y. Zeng, G.P. Simon, H. Wang, Soft Matter 7 (2011) 10048–10056.
[29] X. Cui, Q. Ruan, X. Zhuo, X. Xia, J. Hu, R. Fu, Y. Li, J. Wang, H. Xu, Chem. Rev. 123 (2023) 6891–6952.
[30] X. Zhou, Y. Guo, F. Zhao, G. Yu, Acc. Chem. Res. 52 (2019) 3244–3253.
[31] S.K. Sahoo, B.P. Tripathi, ACS ES&T Engineering 4 (2024) 1644–1656.
[32] P. Banerjee, A. Mukhopadhyay, P. Das, Desalination 451 (2019) 231–240.
[33] D.C. Marcano, D.V. Kosynkin, J.M. Berlin, A. Sinitskii, Z. Sun, A. Slesarev, L. B. Alemany, W. Lu, J.M. Tour, ACS Nano 4 (2010) 4806–4814.
[34] Y. Hartanto, M. Zargar, H. Wang, B. Jin, S. Dai, Environ. Sci. Technol. 50 (2016) 4221–4228.
[35] G. Hakimi, A. Shakeri, M. Yassari, H. Salehi, ACS. App. Polym. Mater 5 (2022) 567–575.
[36] H.G. Schild, Prog. Polym. Sci. 17 (1992) 163–249.
[37] M. Heskins, J.E. Guillet, J. Macromol. Sci. Chem. 2 (1968) 1441–1455.
[38] A. Jangizehi, S. Seiffert, Macromol. Chem. Phys. 223 (2022) 2200070.
[39] Z. Osváth, T. Tóth, B. Iván, Polymer 108 (2017) 395–399.
[40] M.S. Islam, K. Touati, M.S. Rahaman, ACS ES&T Engineering 1 (2021) 467–477.
[41] M. Yassari, A. Shakeri, H. Salehi, Chem. Eng. Res. Design 180 (2022) 369–378.